# Development and validation of the antibodydependent cellular phagocytosis-based signature: A prognostic risk model of gastric cancer

\*Qing Zheng<sup>1,D–F</sup>, \*Zhengi Gong<sup>1,B</sup>, Baizhi Li<sup>1,A–D</sup>, Huaiming Wang<sup>1,A–C</sup>, Shaoxiong Lin<sup>2,F</sup>

- <sup>1</sup> Department of Gastrointestinal Surgery, The First Affiliated Hospital of Shantou University Medical College, China
- <sup>2</sup> Department of Otolaryngology, The First Affiliated Hospital of Shantou University Medical College, China
- A research concept and design; B collection and/or assembly of data; C data analysis and interpretation;
- D writing the article; E critical revision of the article; F final approval of the article

Advances in Clinical and Experimental Medicine, ISSN 1899-5276 (print), ISSN 2451-2680 (online)

Adv Clin Exp Med. 2025;34(3):433-446

#### Address for correspondence

Huaiming Wang E-mail: 17f1hmwang@stu.edu.cn

#### **Funding sources**

This work was supported by grants from Guangdong Basic and Applied Basic Research Foundation (grant No. 2021A1515220075), Shantou Science and Technology Bureau (grant No. 2006241552607), "Dengfeng Project" for the construction of high-level hospitals in Guangdong Province — the First Affiliated Hospital of Shantou University Medical College Supporting Funding (grant No. 202003–17), and Guangdong province Medical ReseFundGrant (grant No. A2022419).

#### **Conflict of interest**

None declared

 $\hbox{*Qing Zheng and Zhenqi Gong contributed equally to this work.}\\$ 

Received on February 24, 2023 Reviewed on March 28, 2024 Accepted on June 11, 2024

Published online on November 18, 2024

#### Cite as

Zheng Q, Gong Z, Li B, Wang H, Lin S. Development and validation of the antibody-dependent cellular phagocytosis-based signature: A prognostic risk model of gastric cancer. Adv Clin Exp Med. 2025;34(3):433—446. doi:10.17219/acem/189914

#### DOI

10.17219/acem/189914

#### Copyright

Copyright by Author(s)
This is an article distributed under the terms of the
Creative Commons Attribution 3.0 Unported (CC BY 3.0)
(https://creativecommons.org/licenses/by/3.0/)

#### **Abstract**

**Background.** Accumulating evidence has supported the effect of antibody-dependent cellular phagocytosis (ADCP) on the tumor microenvironment (TME) and cancer therapy. However, an ADCP-based signature to predict the prognosis of gastric cancer (GC) has not been established.

**Objectives.** We aimed to develop an ADCP-based signature to improve the prognosis prediction of GC.

**Materials and methods.** Antibody-dependent cellular phagocytosis genes that exhibited a differential expression were characterized, followed by the construction and validation of the ADCP-based signature. The potential association between the ADCP-based signature and TME was explored, and the features of the signature genes were investigated. Finally, a predictive nomogram was established based on the ADCP-based signature.

**Results.** Four ADCP-related genes, *MKNK2*, *VCAN*, *LRAT*, and *GNGB*, were identified to construct the ADCP-based signature, and a high ADCP score predicted an unfavorable prognosis in GC patients (p < 0.05). The ADCP-based signature was significantly associated with immune cells, immune checkpoints and immune signaling pathways (p < 0.05). Gastric cancer patients with high ADCP scores benefited less from immunotherapy compared to those with low ADCP scores. A nomogram including age, stage and risk score of the ADCP-based signature was constructed to predict the 1-, 3- and 5-year survival probabilities, with an area under the curve (AUC) of 0.669, 0.675 and 0.685, respectively.

**Conclusions.** The ADCP-based signature may serve as a new option for prognosis prediction and the personalized treatment of GC patients.

**Key words:** bioinformatics analysis, gastric cancer, tumor microenvironment, prognostic signature, antibody-dependent cellular phagocytosis

## **Background**

Gastric cancer (GC) was the 5<sup>th</sup> most diagnosed cancer and the 4<sup>th</sup> most common cause of cancer death in 2020.<sup>1</sup> The incidence and mortality of GC have been reduced in recent years as a result of the prevention and treatment of *Helicobacter pylori* and Epstein–Barr virus (EBV) infections.<sup>2,3</sup> However, the prognosis of GC patients continues to be unsatisfactory due to the impact of locally advanced and distant metastases.<sup>4,5</sup>

Immunotherapy is a promising treatment strategy, but only a fraction of GC patients benefit from it.<sup>6</sup> Also, the immunosuppressive microenvironment of tumors severely reduces the effectiveness of immunotherapy. Therefore, there is a strong need for precise immunotherapy and accurate efficacy prediction using immune-based biomarkers.

Antibody-dependent cellular phagocytosis (ADCP) is the mechanism that leads to the internalization and degradation of target cells through the activation of Fcy receptors on the surface of macrophages to induce phagocytosis.7 It has been shown that the ADCP process can influence the evolution of the tumor microenvironment (TME). A previous study has found that rituximab results in the upregulation of multiple Fcy receptors on macrophages, which correlates with their phagocytic response.8 In addition, anti-KIT antibodies have been observed to inhibit the growth of gastrointestinal stromal tumors by inducing the phagocytosis of macrophages. 9 These studies suggest that ADCP may regulate the progression of different cancers. Hence, it is valuable to examine the role of ADCP-related genes in the progression of GC, as well as establish a relevant prognostic model for the treatment of GC.

In the present research, we conducted bioinformatics approaches to construct and validate an ADCP-based prognostic signature by employing The Cancer Genome Atlas (TCGA) database and the Gene Expression Omnibus (GEO) database. We further explored the role of the ADCP-based signature in the immune microenvironment. Our study can effectively predict the prognosis of GC patients and may provide new perspectives for the treatment of GC.

### **Objectives**

We aimed to develop a robust ADCP-based signature to improve the predicted prognosis of GC.

### **Methods**

### Data collection and processing

RNA-seq data and clinical information on TCGA-STAD were downloaded from the UCSC-Xena platform (https://toil.xenahubs.net), which contained 32 normal tissue samples and 375 tumor tissue samples. The dataset GSE66229

with 300 tumor tissue samples was downloaded from the GEO database for subsequent model validation analysis. A total of 3,405 genes were obtained by downloading ADCP-related genes (Supplementary Table 1) from a study by Kamber et al.<sup>10</sup> and matching them with the above expression profiles. Our workflow is presented in Fig. 1.

# Protein-protein interaction network and functional enrichment analysis

The differential expression analysis of ADCP genes was carried out using the R package DESeq2 (v. 1.36.0, https:// www.bioconductor.org/packages/release/bioc/html/DE-Seq2.html). A false discovery rate (FDR) less than 0.05 and a |log2FoldChange| >1 were selected as the threshold for screening differentially expressed genes. The interaction relationship of the differentially expressed genes was analyzed using the Search Tool for the Retrieval of Interacting Genes/ Proteins (STRING) database (https://cn.string-db.org/) and imported into Cytoscape (v. 3.9.1) to map the protein-protein interaction (PPI) network. Gene Ontology (GO; http://www. geneontology.org) and Kyoto Encyclopedia of Genes and Genomes (KEGG; http://www.genome.ad.jp/kegg) functional enrichment analysis was conducted using the ClusterProfiler package (v. 4.4.4, https://bioconductor.org/packages/release/ bioc/html/clusterProfiler.html).<sup>11</sup>

# Construction and verification of the ADCP-based signature

The 2 datasets from TCGA and GEO were log2-transformed and normalized to obey the same distribution, thus eliminating the effect from different batches. Tumor samples from TCGA-STAD were segregated into a training set and a test set with a 6:4 random split. Samples with survival times less than 30 days were filtered, and a total of 342 tumor tissue samples were finally included. In the training set samples, the differentially expressed genes and the survival information of the samples were merged to identify genes strongly related to the overall prognosis for survival using univariate Cox regression analysis performed with the survival package (v. 3.4-0, https://github.com/therneau/survival).12 The genes were further screened using a 10-fold cross-validation analysis using the executed least absolute shrinkage and selection operator (LASSO) Cox regression model employing the glmnet package (v. 2.0-18, httRiskscore://cran.r-project. org/web/packages/glmnet/index.html).<sup>13</sup> Next, multivariable regression was conducted to further filter the genes. Relying on the gene regression prognostic coefficients and the expression levels of genes in the training set samples, a risk score model was developed; it was derived as follows:

risk score =  $\Sigma$  (Expi × Coefi);

Expi and Coefi represent the expression levels and LASSO regression coefficients of prognostic genes.

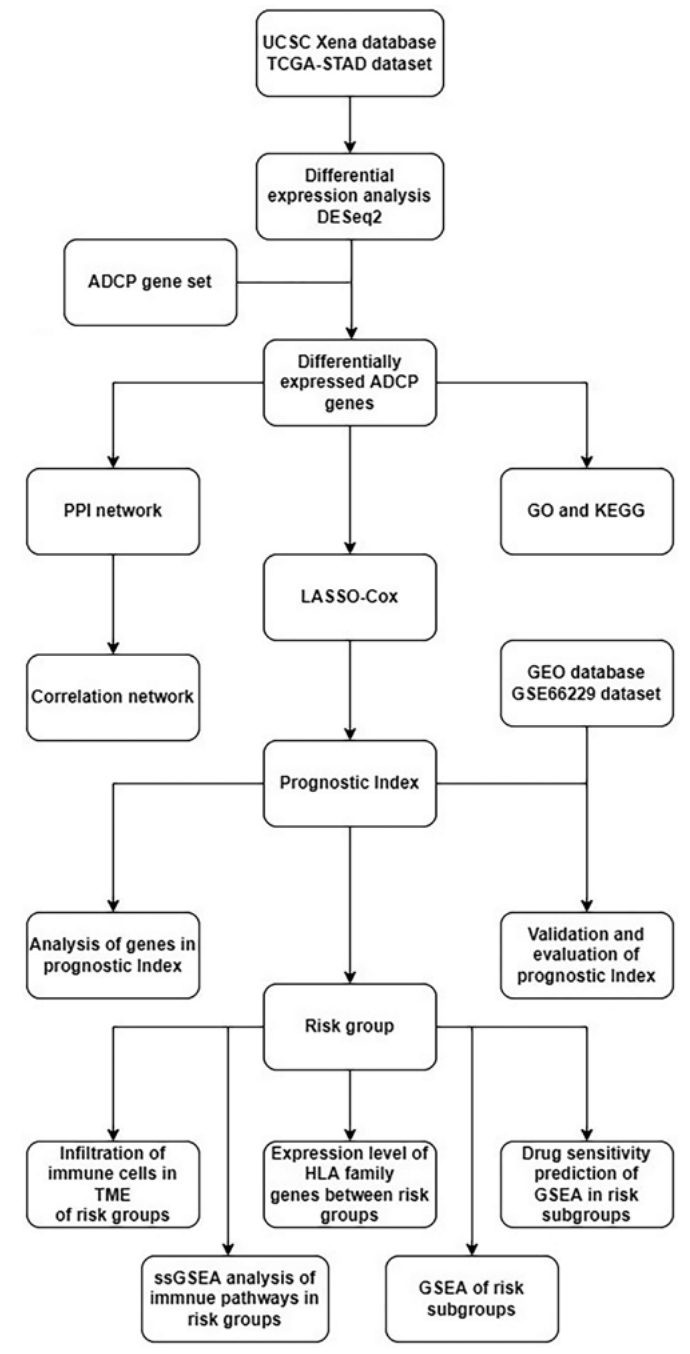


Fig. 1. Study flowchart. Transcriptome data and clinical data were downloaded from TCGA and UCSC Xena. Differential expression analyses were conducted on ADCP-related genes. Protein–protein interaction network and functional enrichment analyses were performed on differentially expressed ADCP-related genes. Four key genes were identified using uni- and multivariable Cox regression as well as the LASSO method to construct an ADCP-based signature. The predictive performance of the ADCP-based signature was validated using GSE66229 from the GEO database. The immune-infiltrating cells, immune pathways and drug sensitivity were explored in risk subgroups defined by the ADCP-based signature

TCGA – The Cancer Genome Atlas; UCSC – University of California Santa Cruz; ADCP – antibody-dependent cellular phagocytosis; PPI – protein-protein interaction; LASSO – Least Absolute Shrinkage and Selection Operator; GEO – Gene Expression Omnibus; STAD – stomach adenocarcinoma; GO – Gene Ontology; KEGG – Kyoto Encyclopedia of Genes and Genomes; TME – tumor microenvironment; HLA – human leukocyte antigen; GSEA – Gene Set Enrichment Analysis; ssGSEA – single-sample Gene Set Enrichment Analysis.

To inspect the correctness of the model, the risk score of each sample from the test set of TCGA and the external validation set of GEO was calculated using the same regression coefficients according to the risk score calculation formula. The samples from the 2 aforementioned validation sets were differentiated based on the median risk score as the cutoff. The overall survival (OS) of each group was assessed using Kaplan–Meier curves. We then plotted the 1-, 3- and 5-year receiver operating characteristic (ROC) curves using the R package survival ROC (v. 1.0.3, https://cran.rstudio.com/web/packages/survivalROC/index.html) and calculated the 1-, 3- and 5-year area under the curve (AUC) values, respectively.

# Prognostic characterization of genes in the model and construction of ceRNA networks

We used the TCGA-STAD dataset for survival analysis of the ADCP-related genes in the signature. The multiMiR package was used to predict gene-associated microRNAs (miRNAs) in the model. Starbase was then used to predict lncRNAs that interact with miRNAs, and the CHEA3 database (https://maayanlab.cloud/chea3) was used to predict transcription factors (TFs) of the model genes. All results were imported into Cytoscape (https://cytoscape.org) to construct a competitive endogenous RNA (ceRNA) network.

# Characteristics of the TME and GSEA in different subgroups

To further examine the immune microenvironment in high- and low-risk groups, Estimation of STromal and Immune cells in MAlignant Tumours using Expression data (ESTIMATE),<sup>14</sup> Cell-type Identification by Estimating Relative Subsets of RNA Transcripts (CIBERSORT), 15 as well as single-sample gene set enrichment analysis (ssGSEA) algorithms were utilized to obtain TME scores and immune cell scores. Moreover, we extracted immune generelated pathways through the immport database (https:// www.immport.org/home). To assess immune pathway variations between high- and low-risk groups, the ssG-SEA algorithm was used to calculate the immune pathway scores of cancer samples. We also captured expression data of human leukocyte antigen (HLA) family genes and immune checkpoint-associated genes to analyze their differential expression in high- and low-risk groups. Gene Set Enrichment Analysis (GSEA) was performed using the ClusterProfiler package (v. 3.18.0)11 to observe significant pathways enriched in the high- and low-risk groups.

# Drug sensitivity and immunotherapy efficacy prediction

The sensitivity of patients to chemotherapeutic agents was evaluated using Genomics of Drug Sensitivity in Cancer

(GDSC; https://www.cancerrxgene.org). <sup>16</sup> The R software package pRRophetic (v. 0.5, https://github.com/paulgeeleher/pRRophetic) was used to determine half-maximal inhibitory concentrations (IC50). We evaluated the differential in drug sensitivity between high- and low-risk groups. The Tumor Immune Dysfunction and Exclusion (TIDE) method was used to predict the benefit of immune checkpoint inhibitor (ICI) treatment in patients with GC.

#### **Construction of nomogram**

Clinical risk models were constructed using univariate and multivariate Cox regression analyses. Next, clinical risk values were calculated for all samples of TCGA-STAD. The prognosis was assessed using Kaplan—Meier curve analysis, and to test the clinical risk model, ROC curves were generated. The calibration curve analysis of the model was assessed using the R package rms (v. 6.3-0, https://hbiostat.org/r/rms). Using the R package dcurves (v. 0.3.0, https://github.com/ddsjoberg/dcurves), decision curve analysis (DCA) decision curves were produced to evaluate the clinical risk model.

#### Statistical analyses

All analyses were conducted in R v. 4.2.1 (R Foundation for Statistical Computing, Vienna, Austria), and a pvalue of 0.05 or less was deemed statistically significant. Univariate and multivariate Cox regression analyses were performed to identify genes and clinical parameters significantly associated with the OS prognosis. Schoenfeld residual plots (conducted by the ggcoxzph function of the survival R package) were used to assess the proportional hazards assumption, which determines whether the effect of the variable on the hazard function is constant over time. The log-rank test was used to compare the differences in survival distributions. A Wilcoxon test was used to compare the differences in medians between samples. The key R-script used in this study can be found in the Supplementary materials.

#### Results

# Differentially expressed ADCP genes and their function in GC

The TCGA dataset was used to obtain the differential expression matrix of GC, which was intersected with ADCP-related genes to obtain 531 differentially expressed ADCP-related genes (238 of them were upregulated and 293 were downregulated, Fig. 2A, Supplementary Table 2). The most significantly up- and downregulated genes were plotted as a heat map (Fig. 2B), with a total of 20 included. These 531 differentially expressed ADCP-related genes were mapped into a PPI network (Fig. 2C, Supplementary

Table 7) through the STRING database. Gene Ontology (Fig. 2D, Supplementary Table 3) and KEGG analysis (Fig. 2E, Supplementary Table 4) were used to explore the functions of the 531 genes. Functional investigation of differentially expressed ADCP-related genes revealed that they were involved in the p53 signaling pathway, PI3K/Akt signaling pathway, calcium signaling pathway, and platinum drug resistance (Fig. 2E), which suggested the possible role of ADCP genes in cancer progression and metastasis.

# Development and validation of ADCP-based signature

Based on the above 531 differential genes, univariate Cox regression was applied using the TCGA-STAD training set to detect 7 prognosis genes (ADAMTS12, MKNK2, VCAN, MMP1, CLDN9, LRAT, and GNG8; Fig. 3A, Supplementary Table 5). The results of the proportional hazards assumption can be found in Supplementary Fig. 1. To further screen the prognostic markers of GC, LASSO regression was employed to identify the prognostic genes acquired from the above univariate Cox regression. The optimal λ was obtained when the partial likelihood of deviance reached the minimum value (Fig. 3B,C). Four prognosisassociated genes (MKNK2, VCAN, LRAT, and GNGB; Fig. 3D, Supplementary Table 6) were available to construct ADCP-related gene signatures after performing multivariate Cox regression. Based on the median risk score, the samples from the training set were separated into a high-risk group (risk score >median risk score) and a low-risk group (risk score ≤median risk score). The ROC curve was plotted to display the 1-, 3- and 5-year AUC for the training set. Validation of the model was conducted in the TCGA test set and the GEO external validation set, indicating a good predictive performance of the model (Fig. 3E). The prognosis differed significantly between the 2 groups, with patients in the high-risk score group presenting a poorer prognosis. In the TCGA-STAD training cohort of 206 GC patients, those with high-risk scores (50%) had a shorter OS (p = 5e-07) than those with low-risk scores (50%). High-risk patients (52.941%) had a shorter OS than low-risk patients (47.059%) across all 136 GC patients in the TCGA-STAD test cohorts (p = 0.003; Fig. 3F). To identify whether or not the ADCP-based signature was reliable, the accuracy of the ADCP-based signature was evaluated using the GEO external validation cohort, with a total of 300 GC patients participating in this study. As seen in Fig. 3F, high-risk patients (49%) had a shorter OS than the low-risk group (51%) (p = 5e-05). The prognostic information of the 4 genes in the signature was demonstrated using a Kaplan-Meier curve, while 3 genes showed significant prognostic value in GC. Between the MKNK2 subgroups, no OS differences were observed (log-rank test, p = 0.151, Fig. 4A). In the VCAN high-expression group, GC patients were found to have a lower survival probability

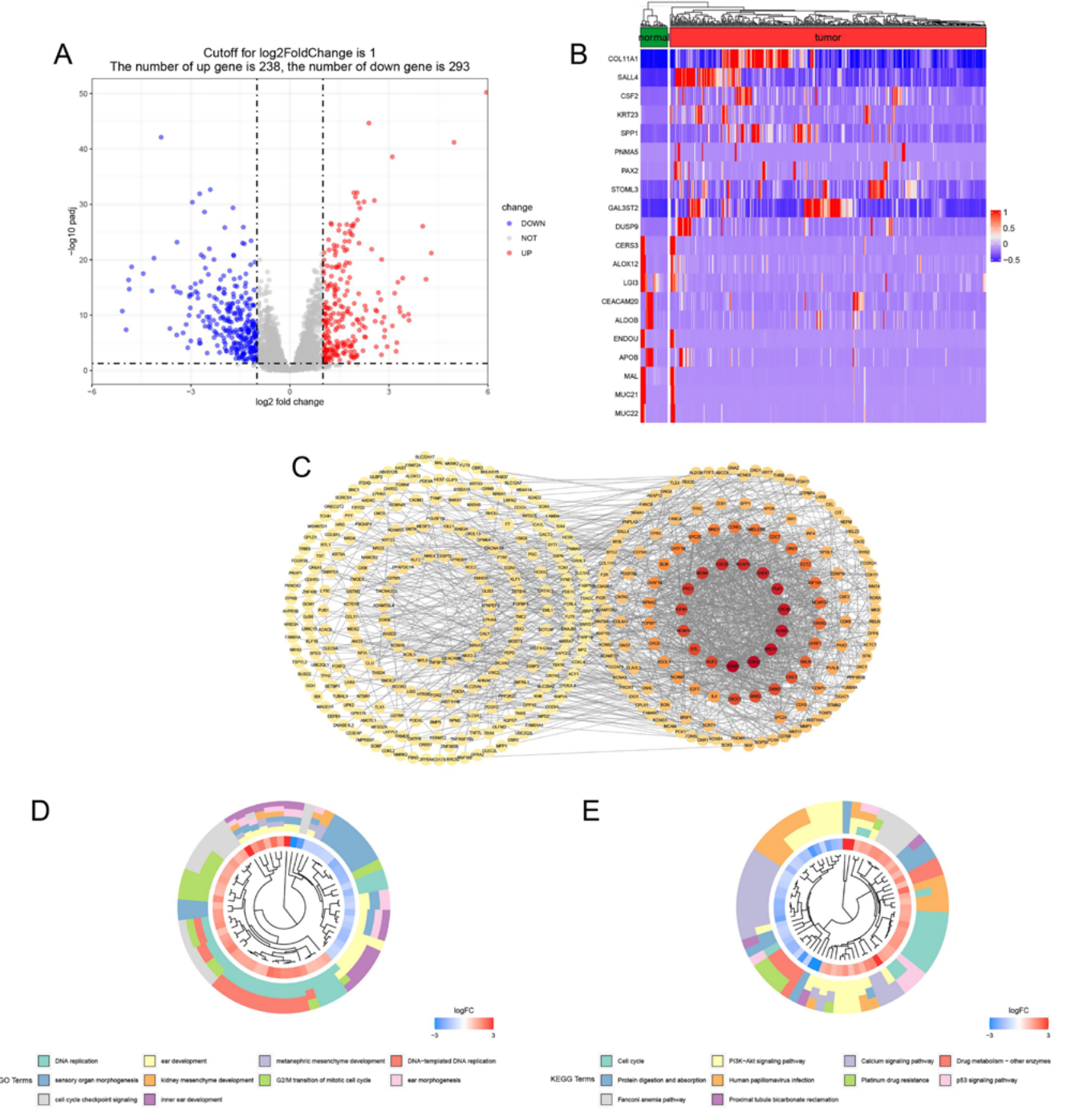


Fig. 2. Identification and characterization of differentially expressed ADCP-related genes. A. A volcano plot representing the 531 differentially expressed ADCP genes (238 of them were upregulated and 293 were downregulated) with a threshold of FDR less than 0.05 and a |log2FC| > 1; B. A heat map containing the 20 most significantly up-and downregulatedADCP genes between normal and tumor samples; C. The PPI network of 531 differentially expressed ADCP-related genes; D–E. GO (D) and KEGG (E) and analysis exploring the functions of the 531 genes

ADCP – antibody-dependent cellular phagocytosis; PPI – protein–protein interaction; FDR – false discovery rate; FC – fold change; GO – Gene Ontology; KEGG – Kyoto Encyclopedia of Genes and Genomes.

(log-rank test, p = 0.027, Fig. 4B). Also, in the LRAT high-expression group, GC patients had a significantly lower OS (log-rank test, p = 0.01, Fig. 4C). The high GNG8 expression group indicated a more favorable prognosis (log-rank test, p = 0.011, Fig. 4D). Based on the 4 genes, 61 miRNAs were predicted using multiR, and 52 lncRNAs were further

predicted with starbase (http://starbase.sysu.edu.cn), followed by the TFs of genes predicted with the CHEA3 database, and the top 10 TFs of meanRank were selected. Genes, miRNAs, lncRNAs, TFs, and interactions between them were imported into Cytoscape to map the ceRNATF network.

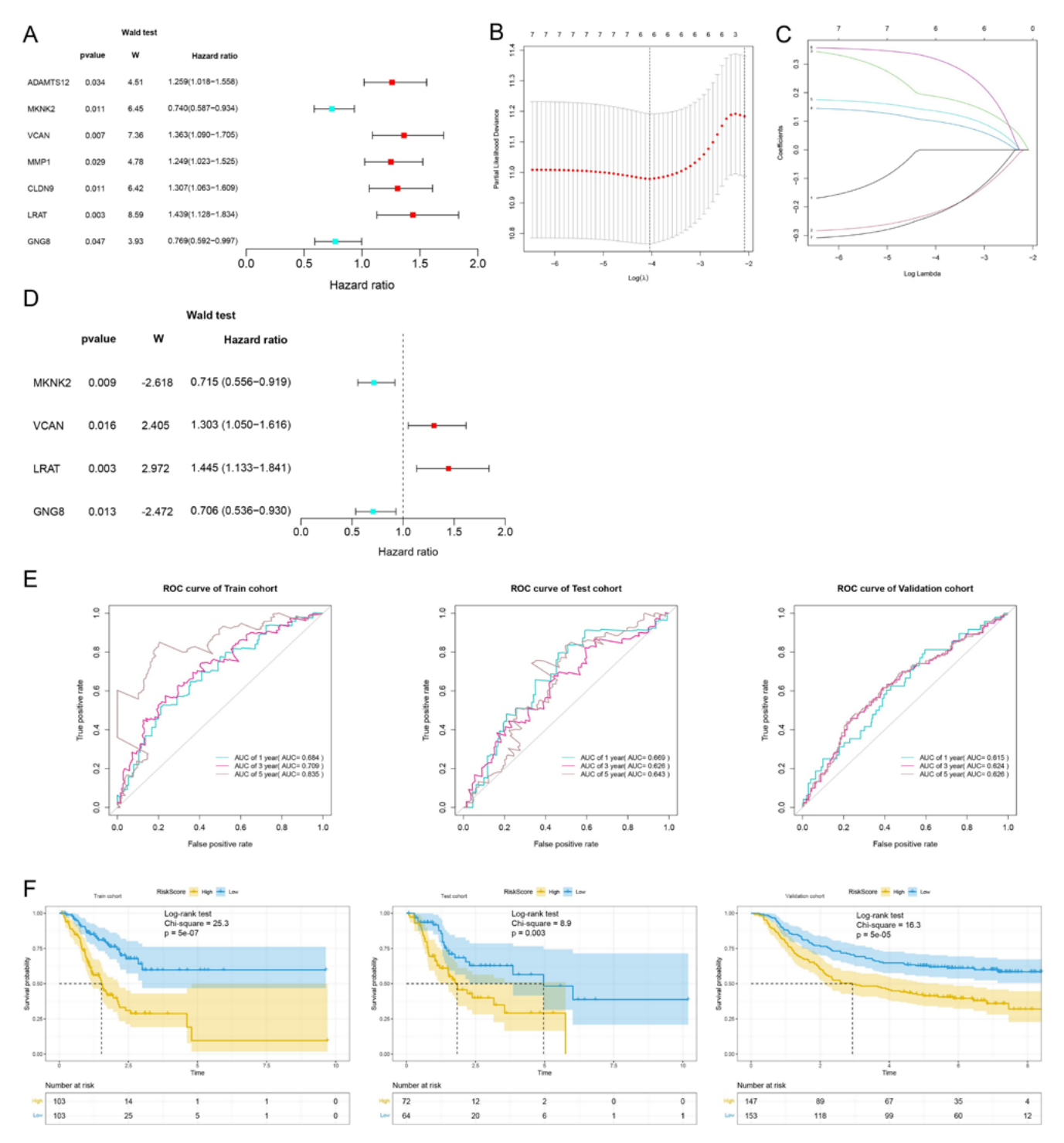


Fig. 3. Construction and validation of an ADCP-based signature. A. Univariate Cox regression analysis identified 7 ADCP-related genes with prognostic value (ADAMTS12, MKNK2, VCAN, MMP1, CLDN9, LRAT, and GNG8); B. Selection of the tuning parameter ( $\lambda$ ) in the least absolute shrinkage and selection operator (LASSO) regression with a 10-fold cross-validation as the minimum criteria; C. LASSO coefficient profiles for clinical features and 6 non-zero coefficients were selected; D. Four genes (MKNK2, VCAN, LRAT, and GNG8) were selected by multivariate Cox regression analysis; E. Receiver operating characteristic (ROC) curves to display the 1-, 3- and 5-year area under the curve (AUC) in the train cohort, test cohort and validation cohort; F. Survival differences between loward high-risk groups in the training cohort (log-rank test, p = 5e-05)

ADCP – antibody-dependent cellular phagocytosis; ADAMTS12 – a disintegrin and metalloproteinase with thrombospondin motifs 12; MKNK2 – threonine kinase 2/MAP kinase interacting serine; VCAN – versican; MMP1 – matrix metallopeptidase 1; CLDN9 – claudin 9; LRAT – lecithin retinol acyltransferase; GNG8 – G protein subunit gamma 8.

Adv Clin Exp Med. 2025;34(3):433-446

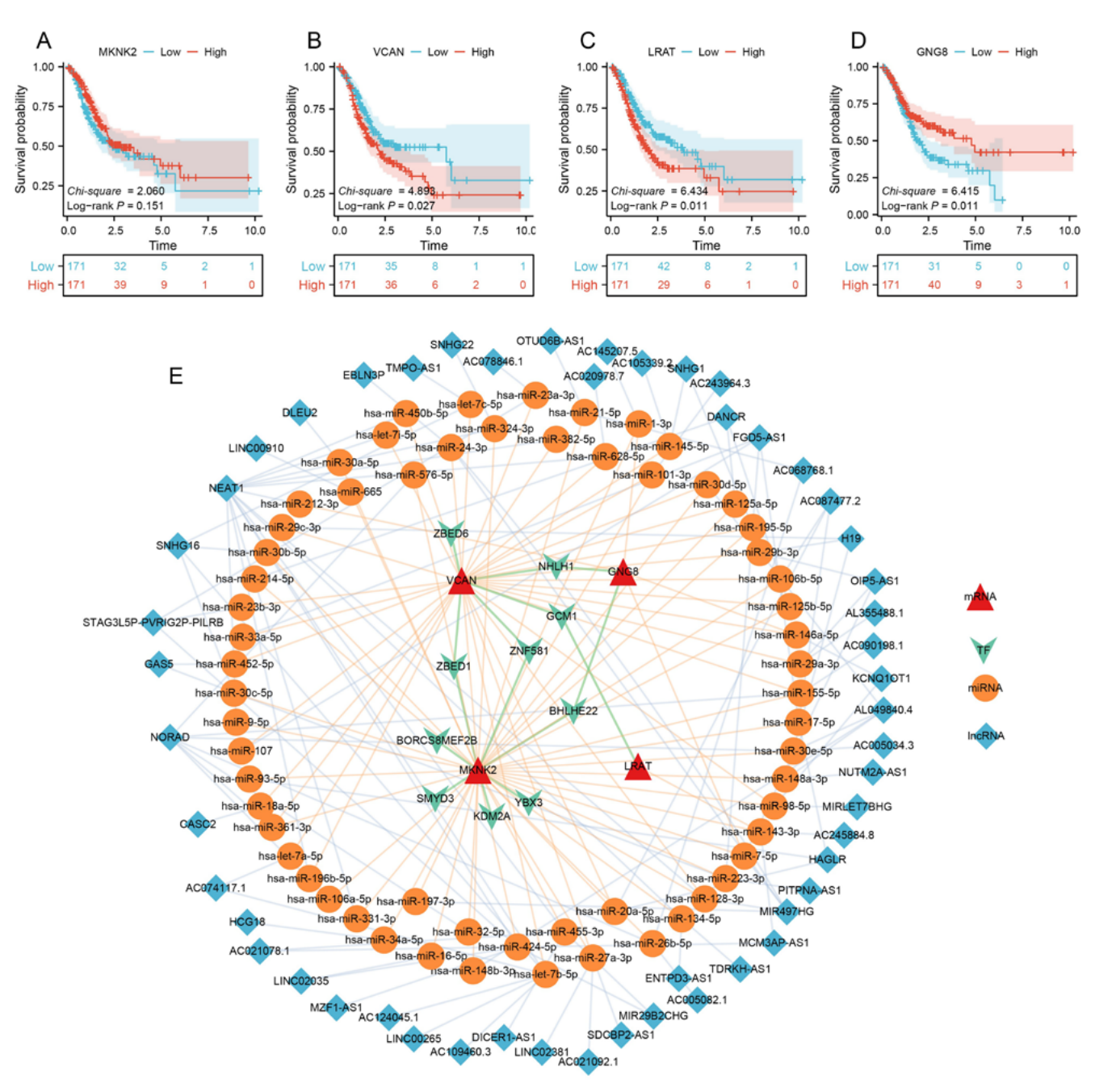


Fig. 4. Survival estimation and PPI network of the signature genes. A–D. Survival differences between low- and high-expression groups of MKNK2 (A) (log-rank test, p = 0.151), VCAN (B) (log-rank test, p = 0.027), LRAT (C) (log-rank test, p = 0.011) and GNG8 (D) (log-rank test, p = 0.011); E. ceRNA-TF network based on the selected genes, miRNAs, lncRNAs, and transcription factors

PPI – protein–protein interaction; MKNK2 – threonine kinase 2/MAP kinase interacting serine; VCAN – versican; LRAT – lecithin retinol acyltransferase; GNG8 – G protein subunit gamma 8; ceRNA – competing endogenous ribonucleic acid; TF – transcription factors; miRNA – microRNA; IncRNA – long noncoding ribonucleic acid.

### **ADCP-based signature in TME**

To gain further insight into the involvement of ADCP-based signature in TME, we used the CIBERSORT (Fig. 5A), ssGSEA (Fig. 5B) and ESTIMATE (Fig. 5C) algorithms to explore the immune infiltration in subgroups. A higher percentage of M2 macrophages was observed in the high-risk score group from the result of CIBERSORT, while T cells CD8+accounted for a smaller percentage compared to the low-risk

score group (Fig. 5A, Supplementary Table 8). The ssGSEA algorithm showed a higher percentage of regulatory T cells (Tregs), as well as a lower percentage of activated CD8+ T cells and activated B cells in the high-risk group (Fig. 5B, Supplementary Table 9). The ESTIMATE algorithm also confirmed the differences in immune infiltration between the high- and low-risk groups (Fig. 5C). In the following work, we analyzed the connection between signature genes and immune cells. As shown in Fig. 5D, VCAN had a significant correlation

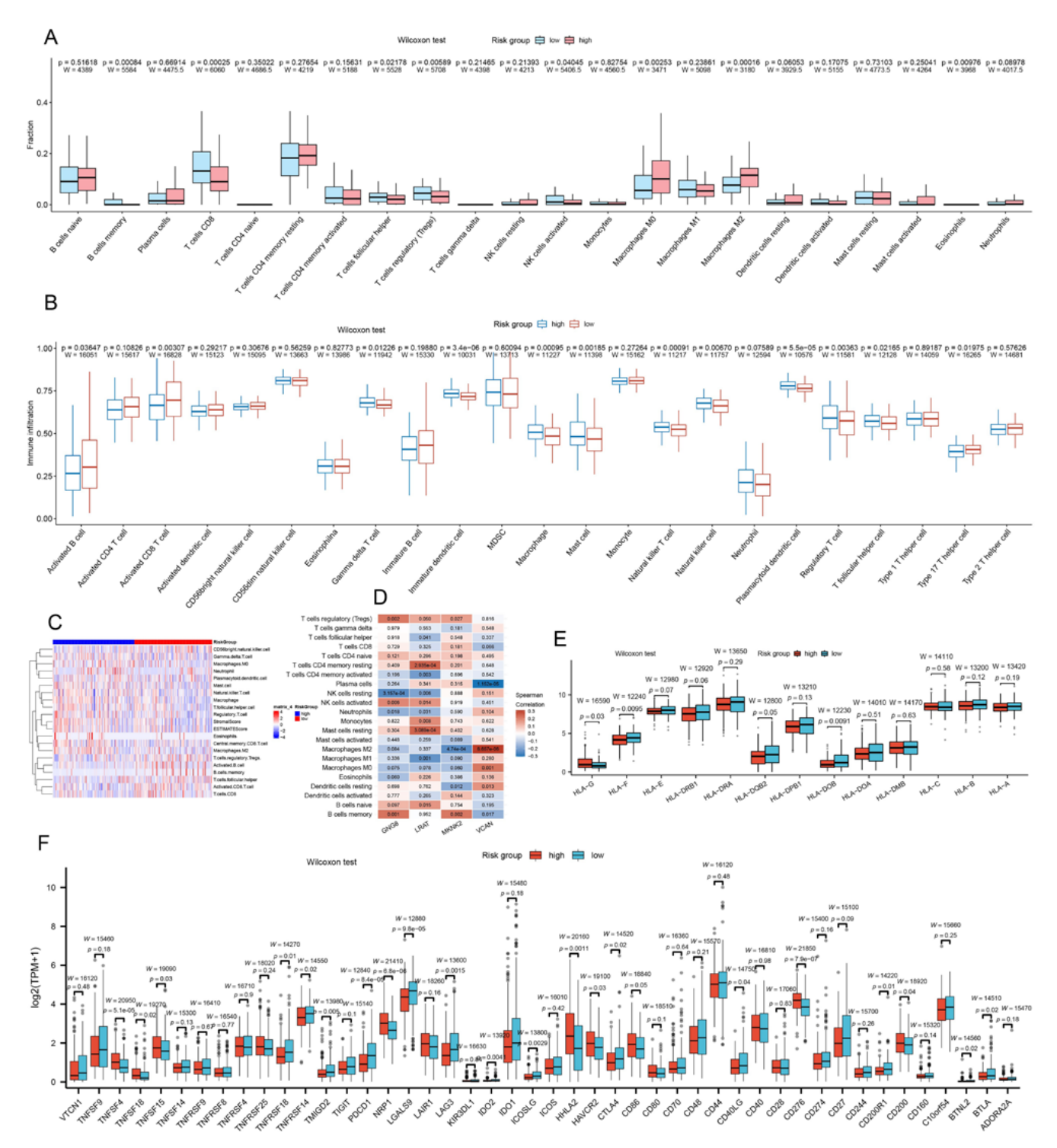


Fig. 5. Immune cell infiltration and immunomodulators of the ADCP-based signature. A,B. Differences in the abundance of immune cell infiltration in high- and low-risk groups using CIBERSORT (A) and ssGSEA (B) algorithms; C. Heat map of immune infiltration between high- and low-risk groups using the CIBERSORT and ESTIMATE algorithms; D. Heat map of the correlation between model genes and differential immune cells using CIBERSORT; E. Differences in the expression of HLA family genes between high- and low-risk groups; F. Differences in the expression of immune checkpoints between high- and low-risk groups

ADCP – antibody-dependent cellular phagocytosis; CIBERSORT – Cell-type Identification by Estimating Relative Subsets of RNA Transcripts; ESTIMATE – Estimation of STromal and Immune cells in MAlignant Tumours using Expression data; ssGSEA – single-sample Gene Set Enrichment Analysis; HLA – human leukocyte antigen.

with M2 macrophages. GNG8 was positively correlated with Tregs and was negatively correlated with activated natural killer cells (Supplementary Table 10). Surprisingly, HLA gene

expression and immune checkpoint gene expression varied significantly across the 2 risk groups (Fig. 5E,F, Supplementary Tables 11,12).

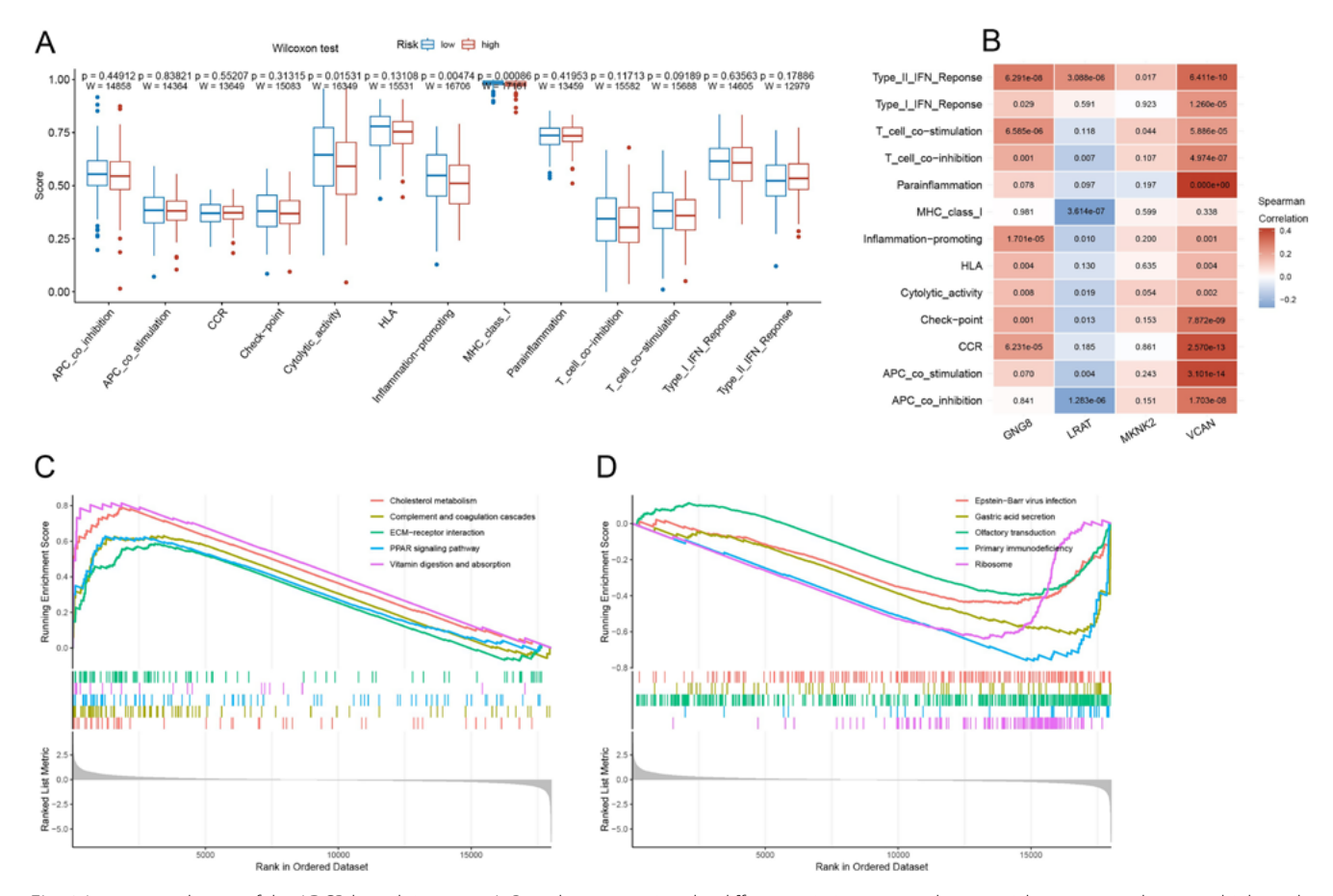


Fig. 6. Immune pathways of the ADCP-based signature. A. Box plots presenting the differences in immune pathway enrichment scores between high- and low-risk groups using ssGSEA; B. Heat map of the correlation between model gene expression and immune pathways using ssGSEA; C,D. High- (C) and low-risk (D) and groups significantly enriched in the different pathways using GSEA

ADCP – antibody-dependent cellular phagocytosis; ssGSEA – single-sample Gene Set Enrichment Analysis; GSEA – Gene Set Enrichment Analysis.

To further characterize the effect of the ADCP-based signature on the TME, we examined the variations of immune pathways between the subgroups. The ssGSEA method was used to provide an estimated value for each cancer sample's immune pathway, which is presented in Fig. 6A and Supplementary Table 13. The association of 4 key genes in the signature with immune-related pathways was also explored (Fig. 6B, Supplementary Table 14). A comparative study of significantly enriched pathways between subgroups was accomplished using GSEA, and the 5 most strongly associated pathways were selected for presentation (Fig. 6C,D, Supplementary Table 15).

# Drug sensitivity and immunotherapy efficacy prediction

As shown in Fig. 7A, patients with high-risk scores exhibited a higher TIDE scoring. Nine compounds with sensitization differences in the high- and low-risk groups were illustrated. In the high-risk group of ADCP-based signatures, the IC50 of GNF.2, Z.LLNle.CHO, AP.24534,

imatinib, NSC.87877, NVP.TAE684, pazopanib, X17.AAG, and PHA.665752 were significantly lower when compared with the low-risk group (Fig. 7B).

#### **Construction of nomogram**

Univariate Cox analysis of the risk score and clinical parameters (age, gender, stage, and grade) demonstrated that age, stage, and risk scores could serve as prognostic factors for GC patients (Supplementary Fig. 2). With additional multivariate Cox regression analysis, a clinical risk model consisting of 3 independent prognostic factors: age, stage and risk score (Fig. 8A) was finally constructed as a nomogram (Fig. 8B). The Kaplan–Meier curve demonstrated that patients with high nomogram scores have a more unfavorable prognosis (Fig. 8C; log-rank test, p = 1.77e-06). The AUC values for 1, 3 and 5 years shown in the ROC curves (Fig. 8D) were 0.669, 0.675 and 0.685, respectively. Calibration curves (Fig. 8E), as well as DCA curves (Fig. 8F), were evaluated for the nomogram, implying it has a good level of predictive accuracy.

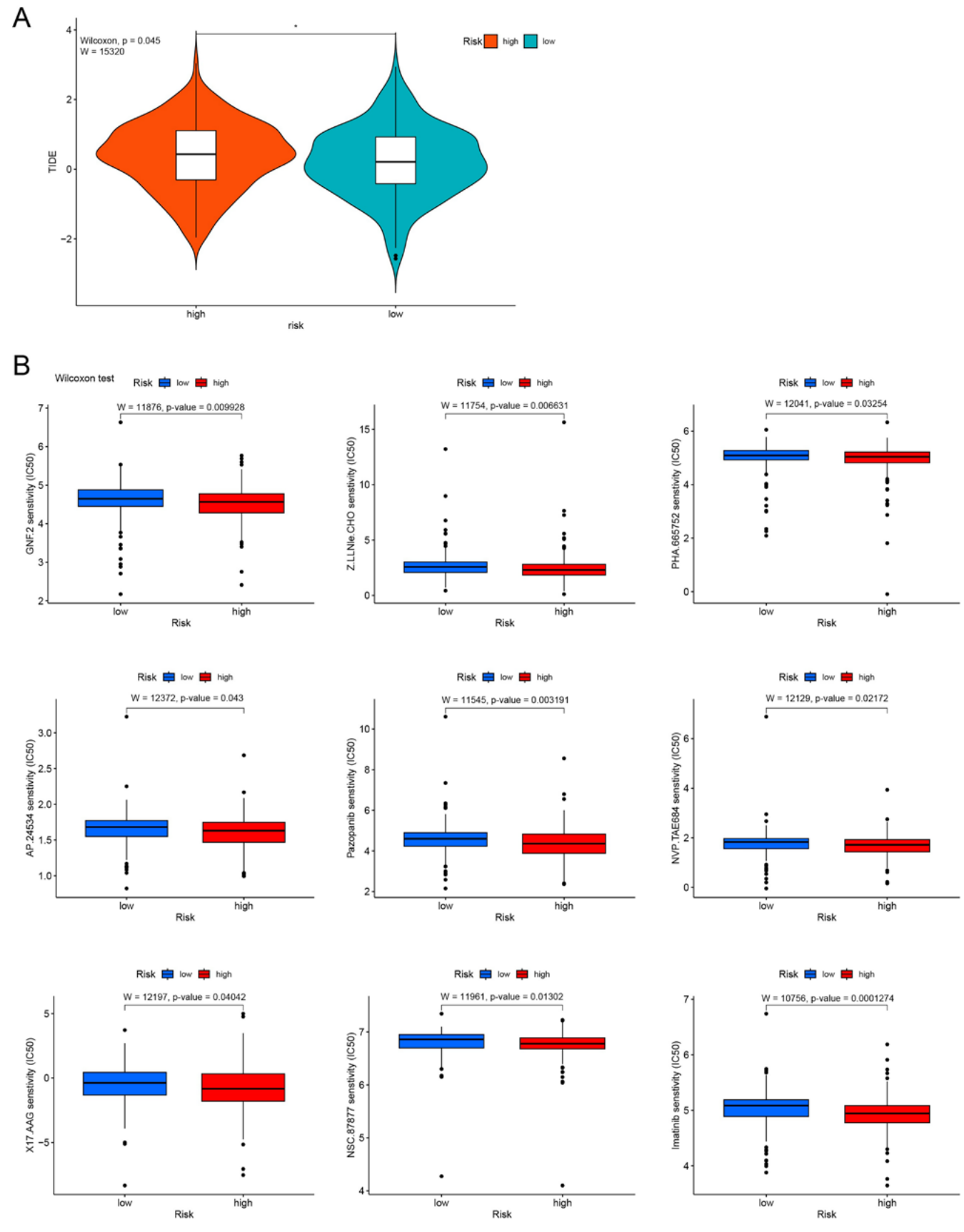


**Fig. 7.** Analyses of drug sensitivity and immunotherapy responses between subgroups. A. The TIDE score was more enriched in the high-risk group; B. The pRRophetic algorithm showed 9 compounds that are more effective for high-risk patients

TIDE – Tumor Immune Dysfunction and Exclusion.

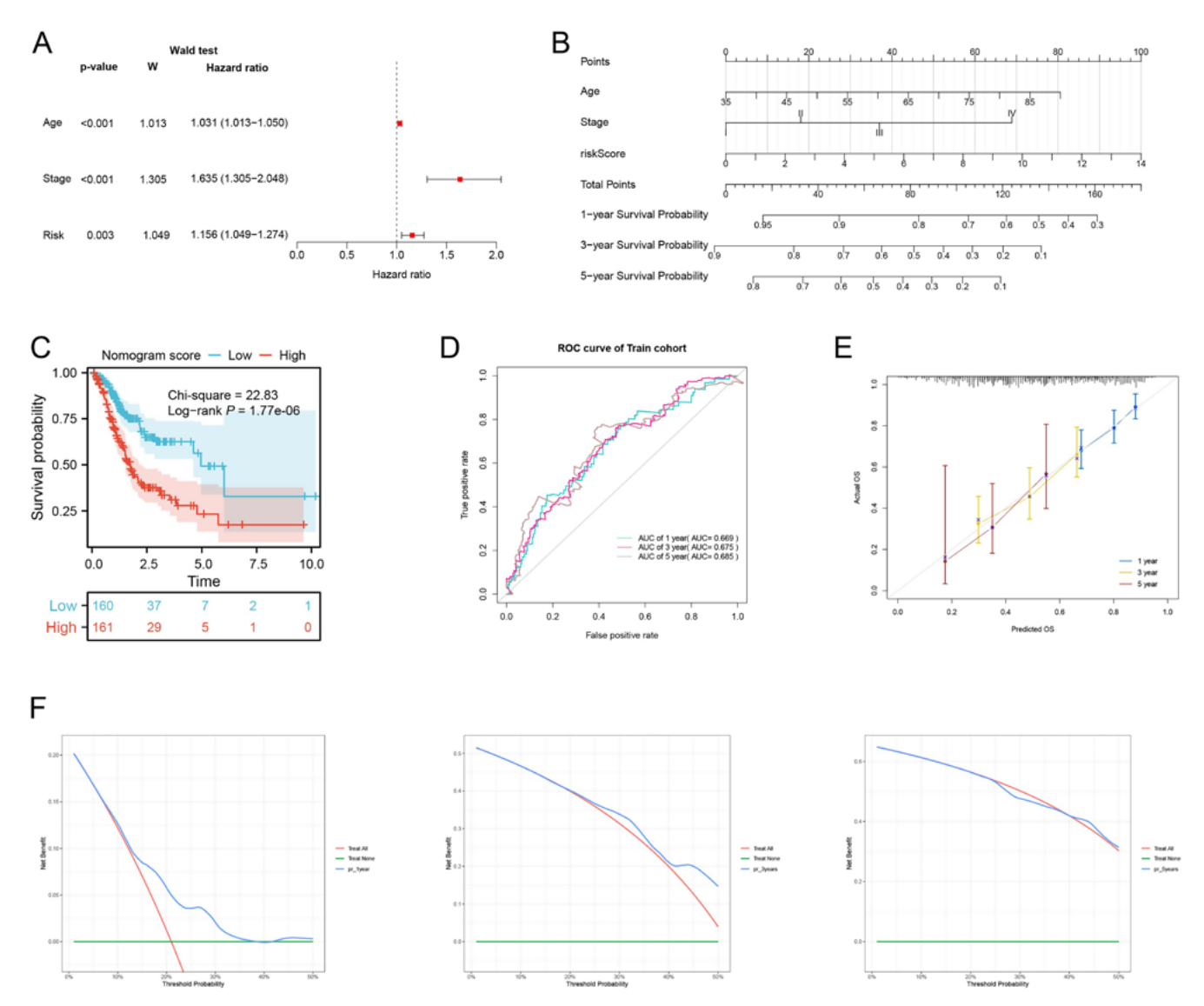


**Fig. 8.** Construction of nomogram. A. Multivariate Cox analysis revealed 3 independent prognostic factors (age, stage and risk score); B. A predictive nomogram based on age, stage and risk score; C. Overall survival estimation of nomogram score subgroups (log-rank test, p = 1.77e-06); D. ROC curves showed that the 1-, 3- and 5-year AUC reached 0.669, 0.675 and 0.685 in the TCGA train cohort, respectively; E. The 1-, 3- and 5-year calibration curves of the nomogram; F. The 1-, 3- and 5-year DCA decision curves of the nomogram.

ROC – receiver operating characteristic; AUC – area under the curve; TCGA – The Cancer Genome Atlas; DCA – decision curve analysis

### **Discussion**

Due to the heterogeneity of GC, the survival durations among patients exhibits huge variation, which covers a range from 5 months to 10 years. <sup>17,18</sup> Patients with early-stage localized GC have a 5-year OS rate above 60%, while in those diagnosed with distant metastasis, it is lower than 5%. <sup>19</sup> Encouragingly, the exploration of reliable biomarkers through bioinformatics has demonstrated remarkable potential in clinical applications. It was recognized that prognostic signatures derived from multiple genes exhibited a significant role in the survival prediction of malignancies. We built an ADCP-based prognostic signature incorporating TCGA data and verified its practicability using the GEO dataset, as well as researching its characteristics with TME. The signature correlates with multiple

immune cells and immune checkpoints. Additionally, differential drug sensitivities and immune efficacies were detected in the subgroups.

The 4 genes in the ADCP-based signature (*MKNK2*, *VCAN*, *LRAT*, and *GNGB*) have been reported in association with the progression of cancer. As in previous studies, *MKNK2* (threonine kinase 2/MAP kinase interacting serine) has been considered an oncogene, which acts as a mediator of various cellular processes to promote the development of prostate cancer and gliomas.<sup>20,21</sup> Furthermore, it has been discovered that *MKNK2* can be targeted by miR-125b, leading to the progression of breast cancer.<sup>22</sup> A previous study also demonstrated that *MKNK2* contributes to the enhancement of chemoresistance of ovarian cancer by inhibiting autophagy through miR-125b.<sup>23</sup> Versican (VCAN) accumulates in tumor cells and

mesenchyme as a protein and is regulated by cytokines. In cancer research, it has been proven that VCAN is involved in the progression of GC. Moreover, VCAN has been recognized as an independent prognostic predictor of GC.<sup>24</sup> Lecithin retinol acyltransferase (LRAT) converts retinol to retinyl esters, regulating cell growth and differentiation.<sup>25</sup> Researchers have demonstrated a significant loss of LRAT expression in invasive bladder cancer, correlating with an increasing tumor stage.<sup>26</sup> G protein subunit gamma 8 (GNG8) participates in chemokine signaling that controls leukocyte migration across the endothelium, which may have a potential implication for the TME.<sup>27</sup>

As research on the TME deepens, the development of new immunotherapy regimens targeting the TME is becoming a major field of interest for cancer treatment. Given that the characteristics of the TME can influence the efficacy of immunotherapy, we focused on the role of ADCP signatures in the TME. The high-risk group of ADCP signatures exhibited a lower probability of survival, resulting from the suppression of the TME. As an important component of the TME, M2 macrophages can secrete undesirable cytokines, thus promoting tumor angiogenesis and tumor metastasis, which is detrimental to patient prognosis. A larger percentage of M2 macrophages was found in the high-risk group, while CD8 T cells, the main contributor that kills tumor cells, displayed a significant proportional decline. Interestingly, there are differential infiltrations of Tregs between the high- and low-risk groups. Tregs are key immune cells with immunosuppressive abilities in the TME, which exert effects through mechanisms such as secreting cytokines, limiting the activation of CD4+ helper T cells and CD8+ cytotoxic T cells, and regulating antigen-presenting cell (APC) functions.  $^{28-33}$  This hinders GC patients from benefiting from ICI therapy. Targeting Tregs holds great potential for reshaping the GC immune microenvironment, enhancing anti-tumor immune responses and improving the OS rate of GC patients. This study stratified GC patients based on ADCP-related genes at the transcriptomic level and also stratified the abundance of Tregs. For GC patients with high Treg activity, traditional ICIs may not be sufficient to fully activate anti-tumor immune responses. In this case, adopting additional strategies to inhibit Treg activities becomes an effective supplementary approach.

Our functional enrichment analysis further suggested that the ADCP model regulates the TME through multiple immune pathways and has a strong immune characteristic. Considering high-risk patients may not benefit as much from immunotherapy, we screened for sensitive and effective compounds for high-risk patients and found that they are more sensitive to pazopanib and imatinib. Notably, imatinib and pazopanib are both tyrosine kinase inhibitors. In addition to the 2 targeted drugs, some chemical drugs were also identified; however, most are limited to cellular experiments. Moreover, traditional cancer chemotherapy based on chemical drugs is prone

to drug resistance and toxic side effects. As an improved form of chemotherapy, metronomic chemotherapy involves administering low doses of drugs continuously without long breaks, which can help avoid these 2 drawbacks. More than 10 years ago, Chinese scholars demonstrated the efficacy and good tolerability of metronomic capecitabine for palliative treatment of advanced GC patients after fluoropyrimidine-based chemotherapy.<sup>34</sup> Furthermore, the good tolerability and potential durable anti-tumor activity of metronomic capecitabine in patients with hepatocellular carcinoma undergoing sorafenib treatment was also confirmed.<sup>35</sup> Mechanistically, metronomic chemotherapy works by inhibiting tumor angiogenesis and inducing immunogenic cell death (ICD), thereby regulating vascular-immune crosstalk. 36 As a result, the combination of metronomic chemotherapy with ICIs has shown synergistic therapeutic effects in preclinical and clinical studies. Especially for high-risk patients, the combination of both may be an effective approach. Unfortunately, metronomic chemotherapy is currently used as a palliative standard care tool. Utilizing bioinformatic methods to identify biomarkers can benefit metronomic chemotherapy and may expand the role of metronomic chemotherapy in cancer therapy.

To more accurately exploit the predictive ability of the ADCP signature, we combined univariate and multivariate analysis with Cox regression and eventually constructed a nomogram selecting age, stage and risk scores. This nomogram visualized the logistic regression model to facilitate rapid clinical judgment on the prognosis of GC patients. The AUC curve demonstrated that the model predicted the prognosis of GC patients with reliable accuracy. The calibration curve illustrates that the predicted probability of patient survival is in good agreement with the actual probability, and its clinical application can be attempted.

#### Limitations

Despite the fact that this research made some contributions, it did have several shortcomings. First, although our work evaluated high sample sizes of GC cohorts to construct a well-validated prognostic signature, the use of diverse platforms might generate sampling bias, which may induce some ambiguity in the assessments of gene expression. Second, the underlying mechanisms by which the 4 genes (MKNK2, VCAN, LRAT, and GNGB) that were combined into the ADCP signature in our investigation contributed to GC progression, and the unfavorable outcome still remains unexplained; additional in-depth research into their biological functions might generate fresh targets and therapeutic strategies. Third, recognizing that these cohorts are merely retrospective, more prospective clinical studies are necessary to confirm our results. In particular, future research needs to evaluate the predictive function of the ADCP signature throughout both prognosis and the responsiveness to different kinds of treatment interventions. Finally, the accuracy of CIBER-SORT and ssGSEA is limited by the representativeness of the training data and the assumptions of the algorithms themselves, leading to biases in assessing the levels of immune cell infiltration. These 2 algorithms mainly focus on the composition and proportion of immunocytes, with limited evaluation of their functional states. This calls for the adoption of more validated algorithms to analyze immunocytes and to compare algorithm performance through methods like cross-validation. Additionally, integrating multi-omics data, including gene expression, proteomics and metabolomics data, is essential for inferring the functional states of immune cells.

#### **Conclusions**

We identified 4 prognosis-associated genes that were related to OS and the TME in GC by also constructing a model with strong predictive effects. To the best of our knowledge, this report is the first effort to develop a prognostic signature of ADCP-related genes for GC. Our study offers a novel option for the diagnosis and prediction of GC and may contribute new biomarkers for the treatment of GC.

### **Ethical approval**

This article does not contain any studies with human participants or animals performed by any of the authors. Therefore, no ethical approval or consent was required. No administrative permission and/or licenses were acquired for this study to access the original data used in this research.

#### Supplementary data

The Supplementary materials are available at https://doi.org/10.5281/zenodo.11065549. The package includes the following files:

Supplementary Fig. 1. Proportional hazards assumption based on Schoenfeld's global and individual test. (A–D) The p-values of the Schoenfeld's global test are all greater than 0.05 in gene selection using univariate Cox regression (A) and multivariate Cox regression (B), selection of ADCP-based signature and clinical features using univariate cox regression (C), and multivariate Cox regression (D).

Supplementary Fig. 2. Selection of ADCP-based signature and clinical parameters using univariate Cox regression.

Supplementary Table 1. Antibody-dependent cellular phagocytosis-related genes.

Supplementary Table 2. 531 differentially expressed antibody-dependent cellular phagocytosis-related genes. Supplementary Table 3. Results of GO.

Supplementary Table 4. Results of KEGG.

Supplementary Table 5. Selection of antibody-dependent cellular phagocytosis-related genes with prognostic value using univariate Cox regression analysis.

Supplementary Table 6. Selection of antibody-dependent cellular phagocytosis-related genes with prognostic value using multivariate Cox regression analysis.

Supplementary Table 7. Node information of protein-protein interactions.

Supplementary Table 8. Wilcoxon test results of immunocyte infiltration between risk subgroups using CIBERSORT.

Supplementary Table 9. Wilcoxon test results of immunocyte infiltration between risk subgroups using ssGSEA.

Supplementary Table 10. Spearman correlation results of immunocyte infiltration and signature genes using CIBERSORT.

Supplementary Table 11. Wilcoxon test results of HLA gene expression between risk subgroups.

Supplementary Table 12. Wilcoxon test results of immune checkpoint expression between risk subgroups.

Supplementary Table 13. Wilcoxon test results of immune pathways between risk subgroups using ssGSEA.

Supplementary Table 14. Spearman correlation results of immune pathways and signature genes using ssGSEA.

Supplementary Table 15. GSEA results between risk subgroups.

### **Data availability**

The datasets generated and/or analyzed during the current study are available from the corresponding author on reasonable request.

#### **Consent for publication**

Not applicable.

#### **ORCID** iDs

#### References

- Boorjian S, Tickoo SK, Mongan NP, et al. Reduced lecithin. Clin Cancer Res. 2004;10(10):3429–3437. doi:10.1158/1078-0432.CCR-03-0756
- Campbell C, Rudensky A. Roles of regulatory T cells in tissue pathophysiology and metabolism. *Cell Metab*. 2020;31(1):18–25. doi:10.1016 /j.cmet.2019.09.010
- Chen W, Zheng R, Baade PD, et al. Cancer statistics in China, 2015. CA Cancer J Clin. 2016;66(2):115–132. doi:10.3322/caac.21338
- Cuadrado E, Van Den Biggelaar M, De Kivit S, et al. Proteomic analyses of human regulatory T cells reveal adaptations in signaling pathways that protect cellular identity. *Immunity*. 2018;48(5):1046–1059.e6. doi:10.1016/j.immuni.2018.04.008
- Edris B, Willingham SB, Weiskopf K, et al. Anti-KIT monoclonal antibody inhibits imatinib-resistant gastrointestinal stromal tumor growth. Proc Natl Acad Sci U S A. 2013;110(9):3501–3506. doi:10.1073/pnas. 1222893110

- 6. Friedman J, Hastie T, Tibshirani R, et al. LASSO and elastic-net regularized generalized linear models. Pasadena, USA: Stanford University; 2023. https://glmnet.stanford.edu. Accessed January 6, 2023.
- Gao JP, Xu W, Liu WT, Yan M, Zhu ZG. Tumor heterogeneity of gastric cancer: From the perspective of tumor-initiating cell. World J Gastroenterol. 2018;24(24):2567–2581. doi:10.3748/wjg.v24.i24.2567
- Geeleher P, Cox N, Huang RS. pRRophetic: An R Package for prediction of clinical chemotherapeutic response from tumor gene expression levels. *PLoS One*. 2014;9(9):e107468. doi:10.1371/journal.pone. 0107468
- Granito A, Marinelli S, Terzi E, et al. Metronomic capecitabine as second-line treatment in hepatocellular carcinoma after sorafenib failure. *Digest Liver Dis*. 2015;47(6):518–522. doi:10.1016/j.dld.2015.03.010
- Kamber RA, Nishiga Y, Morton B, et al. Inter-cellular CRISPR screens reveal regulators of cancer cell phagocytosis. *Nature*. 2021;597(7877): 549–554. doi:10.1038/s41586-021-03879-4
- He S, Shen J, Hong L, Niu L, Niu D. Capecitabine "metronomic" chemotherapy for palliative treatment of elderly patients with advanced gastric cancer after fluoropyrimidine-based chemotherapy. *Med Oncol.* 2012;29(1):100–106. doi:10.1007/s12032-010-9791-x
- Kamen L, Myneni S, Langsdorf C, et al. A novel method for determining antibody-dependent cellular phagocytosis. *J Immunol Methods*. 2019;468:55–60. doi:10.1016/j.jim.2019.03.001
- Leidi M, Gotti E, Bologna L, et al. M2 macrophages phagocytose rituximab-opsonized leukemic targets more efficiently than M1 cells in vitro. J Immunol. 2009;182(7):4415–4422. doi:10.4049/jimmunol. 0713732
- Li MO, Rudensky AY. T cell receptor signalling in the control of regulatory T cell differentiation and function. *Nat Rev Immunol*. 2016; 16(4):220–233. doi:10.1038/nri.2016.26
- Li W, Han F, Fu M, Wang Z. High expression of VCAN is an independent predictor of poor prognosis in gastric cancer. J Int Med Res. 2020;48(1):030006051989127. doi:10.1177/0300060519891271
- Liu B, Sun Y, Tang M, et al. The miR-361-3p increases enzalutamide (Enz) sensitivity via targeting the ARv7 and MKNK2 to better suppress the Enz-resistant prostate cancer. *Cell Death Dis*. 2020;11(9):807. doi:10.1038/s41419-020-02932-w
- Mogilevsky M, Shimshon O, Kumar S, et al. Modulation of MKNK2 alternative splicing by splice-switching oligonucleotides as a novel approach for glioblastoma treatment. Nucl Acids Res. 2018;46(21): 11396–11404. doi:10.1093/nar/gky921
- Muraro E, Vinante L, Fratta E, et al. Metronomic chemotherapy: Antitumor pathways and combination with immune checkpoint inhibitors. *Cancers (Basel)*. 2023;15(9):2471. doi:10.3390/cancers15092471
- Newman AM, Liu CL, Green MR, et al. Robust enumeration of cell subsets from tissue expression profiles. *Nat Methods*. 2015;12(5):453–457. doi:10.1038/nmeth.3337
- 20. Newton R, Priyadharshini B, Turka LA. Immunometabolism of regulatory T cells. *Nat Immunol.* 2016;17(6):618–625. doi:10.1038/ni.3466

- Sakaguchi S, Mikami N, Wing JB, Tanaka A, Ichiyama K, Ohkura N. Regulatory T cells and human disease. *Annu Rev Immunol*. 2020;38(1): 541–566. doi:10.1146/annurev-immunol-042718-041717
- 22. Shah MA, Ajani JA. Gastric cancer: An enigmatic and heterogeneous disease. *JAMA*. 2010;303(17):1753. doi:10.1001/jama.2010.553
- 23. Sheren-Manoff M, Shin SJ, Su D, Bok D, Rando RR, Gudas LJ. Reduced lecithin:retinol acyltransferase expression in human breast cancer. *Int J Oncol.* 2006;29(5):1193–1199. PMID:17016651.
- Sillé FCM, Thomas R, Smith MT, Conde L, Skibola CF. Post-GWAS functional characterization of susceptibility variants for chronic lymphocytic leukemia. *PLoS One*. 2012;7(1):e29632. doi:10.1371/journal.pone.0029632
- Smyth EC, Nilsson M, Grabsch HI, Van Grieken NC, Lordick F. Gastric cancer. Lancet. 2020;396(10251):635–648. doi:10.1016/S0140-6736 (20)31288-5
- Sung H, Ferlay J, Siegel RL, et al. Global cancer statistics 2020: GLO-BOCAN estimates of incidence and mortality worldwide for 36 cancers in 185 countries. CA Cancer J Clin. 2021;71(3):209–249. doi:10.3322/caac.21660
- Therneau T, Lumley T. Package Survival: A package for Survival Analysis in R. R Package. Version 2, 38. Comprehensive R Archive Network (CRAN); 2024. https://vps.fmvz.usp.br/CRAN/web/packages/survival/survival.pdf. Accessed January 6, 2023.
- Van Cutsem E, Sagaert X, Topal B, Haustermans K, Prenen H. Gastric cancer. *Lancet*. 2016;388(10060):2654–2664. doi:10.1016/S0140-6736(16)30354-3
- Van Der Veeken J, Gonzalez AJ, Cho H, et al. Memory of inflammation in regulatory T cells. *Cell*. 2016;166(4):977–990. doi:10.1016/j.cell. 2016.07.006
- 29. Wang J, Da C, Su Y, Song R, Bai Z. MKNK2 enhances chemoresistance of ovarian cancer by suppressing autophagy via miR-125b. *Biochem Biophys Res Commun*. 2021;556:31–38. doi:10.1016/j.bbrc.2021.02.084
- 31. Wang Y, Zhang X, Ding J, Chao Z, Dress A, Lai L. MKNK2 is a valid target of miR-125b in breast cancer. *Gene Reports*. 2016;5:92–97. doi:10.1016/j.genrep.2016.09.008
- 32. Wu T, Hu E, Xu S, et al. clusterProfiler 4.0: A universal enrichment tool for interpreting omics data. *Innovation (Camb)*. 2021;2(3):100141. doi:10.1016/j.xinn.2021.100141
- 33. Yoshihara K, Shahmoradgoli M, Martínez E, et al. Inferring tumour purity and stromal and immune cell admixture from expression data. *Nat Commun*. 2013;4(1):2612. doi:10.1038/ncomms3612
- Yuan L, Xu ZY, Ruan SM, Mo S, Qin JJ, Cheng XD. Long non-coding RNAs towards precision medicine in gastric cancer: Early diagnosis, treatment, and drug resistance. Mol Cancer. 2020;19(1):96. doi:10.1186/ s12943-020-01219-0
- 35. Zhao Q, Cao L, Guan L, et al. Immunotherapy for gastric cancer: Dilemmas and prospect. *Brief Funct Genomics*. 2019;18(2):107–112. doi:10.1093/bfgp/ely019
- Zong L, Abe M, Seto Y, Ji J. The challenge of screening for early gastric cancer in China. *Lancet*. 2016;388(10060):2606. doi:10.1016/S0140-6736(16)32226-7